Atmos. Chem. Phys. Discuss., 14, 8723–8752, 2014
www.atmos-chem-phys-discuss.net/14/8723/2014/
doi:10.5194/acpd-14-8723-2014

Atmospheric Chemistry and Physics Discussions

Origin, variability and age of biomass burning plumes intercepted during BORTAS-B

D. P. Finch[1], **P. I. Palmer**[1], **and M. Parrington**[1,*]

[1]School of GeoSciences, University of Edinburgh, UK
[*]now at: the European Centre for Medium-range Weather Forecasts, Reading, UK

Received: 14 February 2014 – Accepted: 7 March 2014 – Published: 31 March 2014

Correspondence to: D. P. Finch (d.finch@ed.ac.uk)

Published by Copernicus Publications on behalf of the European Geosciences Union.

Abstract

We use the GEOS-Chem atmospheric chemistry transport model to interpret aircraft measurements of carbon monoxide (CO) in biomass burning outflow taken during the 2011 BORTAS-B campaign over eastern Canada. The model has some skill reproducing the observed variability ($r = 0.45$) but has a negative bias for observations below 100 ppb and a positive bias above 300 ppb. We find that observed CO variations are largely due to NW North American biomass burning, as expected, with smaller and less variable contributions from fossil fuel combustion from eastern Asia and NE North America. To help interpret observed variations of CO we develop an Eulerian effective age of emissions ($\overline{A}$) metric, accounting for mixing and chemical decay, which we apply to pyrogenic emissions of CO. We find that during BORTAS-B the age of emissions intercepted over Halifax, Nova Scotia is typically 4–11 days, and on occasion as young as two days. We show that $\overline{A}$ is typically 1–5 days older than the associated photochemical ages inferred from colocated measurements of different hydrocarbons. We find that the median difference between the age measures ($\Delta\tau$) in plumes ($CH_3CN > 150$ ppt) peaks at 3–5 days corresponding to a chemical retardation of 50 %. We find a strong relationship in plumes between $\overline{A}$ and $\Delta\tau$ ($r^2 = 0.60$), which is not evident outwith these plumes ($r^2 = 0.23$). We argue that these observed relationships, together with a robust observed relationship between CO and black carbon aerosol during BORTAS-B ($r^2 > 0.7$), form the basis of indirect evidence that aerosols co-emitted with gases during pyrolysis markedly slowed down the plume photochemistry during BORTAS-B with respect to photochemistry at the same latitude and altitude in clear skies.

1 Introduction

The open burning of biomass is an inefficient combustion process, resulting in the release of a wide range of chemically reactive gases and particles that contribute to the production of ozone in the troposphere (Goode et al., 2000; Koppmann et al., 2005;

ACPD
14, 8723–8752, 2014

Akagi et al., 2011), with implications for national surface air quality and air quality mitigation strategies. However, the rate and extent of photochemical ozone production in biomass burning outflow is still a matter of debate that largely reflects the sensitivity of results to environmental conditions (Jaffe and Wigder, 2012). In this paper we present an analysis of measurements of carbon monoxide (CO) from the BORTAS-B aircraft campaign during July 2011 (Palmer et al., 2013), in conjunction with a 3-D chemistry transport model to understand the processes that determine observed CO variability and relate the ages of emissions to the observed photochemical production of ozone.

The main source of CO is from the incomplete combustion of fossil fuel, biomass, and biofuel. There is also a source of CO from the oxidation from methane and non-methane volatile organic compounds (NMVOCs) (Duncan et al., 2007). The main sink is from the oxidation by the hydroxyl radical (OH), resulting in an atmospheric lifetime of weeks to months depending on latitude and season. We use airborne CO measurements from phase B of the Quantifying the impacts of BOReal forest fires on Tropospheric oxidants over the Atlantic using Aircraft and Satellites (BORTAS-B) project, July 2011. The overall objective of BORTAS was to better understand the production of tropospheric ozone in respect to the chemical evolution of plumes from boreal forest fires, which was achieved by integrating aircraft (Lewis et al., 2013; Le Breton et al., 2013; O'Shea et al., 2013), surface (Gibson et al., 2013; Griffin et al., 2013), sonde (Parrington et al., 2012), and satellite measurements (Tereszchuk et al., 2013) of atmospheric composition. Phase A of BORTAS was conducted without aircraft in July 2010 (Parrington et al., 2012).

In the next section we briefly describe the CO data we analyse. The GEOS-Chem chemistry transport model is described in Sect. 3, including a description of a new age of emission calculation which we use to interpret the data. Our results are reported in Sect. 4, including a statistical analysis of the data and a model interpretation of the data. We conclude in Sect. 5.

ACPD
14, 8723–8752, 2014

2 Data and methods

2.1 BORTAS-B carbon monoxide and CH_3CN data

Here we use data exclusively from the BORTAS-B aircraft campaign. The focus of the work shown here is the analysis of CO measurements, which are operated by the Facility for Airborne Atmospheric Measurements on the BAe-146 atmospheric research aircraft using a fast-response vacuum-UV resonance fluorescence instrument (Gerbig et al., 1999). The instrument has an averaging time of 1 s and a precision and accuracy of 1 ppb and 3 %, respectively. We use measurements of acetonitrile (CH_3CN, not shown), an additional tracer of biomass burning, measured by Proton Transfer Reaction Mass Spectrometer (Murphy et al., 2010) to isolate plumes within BORTAS-B. These measurements have a mean precision of 37 ppt during BORTAS-B (Palmer et al., 2013). We define plumes as CO measurements corresponding to $CH_3CN > 150$ ppt.

2.2 The GEOS-Chem atmospheric chemistry model

We use the GEOS-Chem atmospheric chemistry model (www.geos-chem.org) to interpret the BORTAS-B CO measurement. The model has been documented extensively (e.g., Bey et al., 2001; Duncan et al., 2007; Gonzi et al., 2011; Parrington et al., 2012) and here we only include those details relevant to our study.

We use v9-01-03 of the model, driven by GEOS-5 assimilated meteorological data from the NASA Global Modelling and Assimilation Office (GMAO) Goddard Earth Observing System (GEOS). For all calculations reported here we use a spatial resolution of 2° latitude by 2.5° longitude (a degradation of the native resolution of 0.5° × 0.667°) with 47 vertical levels with a temporal resolution of three hours. We use the Global Fire Emissions Database (GFED-3), describing biomass burning emissions (Giglio et al., 2010), which has a three-hour temporal resolution; fossil fuel emissions from the Emissions Database for Global Atmospheric Research (EDGAR, Olivier et al., 1999); and

ACPD
14, 8723–8752, 2014

biogenic emissions from the Model of Emissions of Gases and Aerosol from Nature (MEGAN, Guenther et al., 2006). We report model calculations from the summers (JJA) of 2008–2011. We initialize the model in 2007, using previous model output, and run using a single total CO tracer for 9 months until our study period JJA 2008. During the summer periods we use "tagged" tracers (described below) and between the successive summer periods we collapse these tagged tracers back to the single tracer for computational expediency.

For the CO attribution calculations, we use a "tagged" version of the model (e.g., Jones et al., 2003; Palmer et al., 2003, 2006; Feng et al., 2009; Fisher et al., 2010), which uses pre-calculated monthly 3-D OH fields. Using these fields allows us to linearly decompose the CO originating from specific processes and geographical regions. Figure 1 shows the geographical regions we use. For biomass burning in the Northern Hemisphere we split North America into four quadrants, consider Europe as one region, and split Russia/Siberia into three regions (western, mid, and eastern). We show below that most of the observed CO over eastern Canada during JJA originates from these regions. For Northern Hemisphere fossil fuel we have combined some regions that do not play a significant role in the interpretation of the BORTAS-B data. The chemical source of CO from the oxidation of methane and NMVOCs is treated as one global tracer. In total, we have 28 tracers (including the background) that sum to the total atmospheric CO. Wherever we compare the model against data we sample the model at the time and location of the measurement.

2.3 Age of emission model calculation

We use the same model structure for the "tagged" CO simulation to calculate the age of air. To calculate the age of emissions we adapt the model to instead emit an arbitrary constant amount to a day-specific tracer wherever there is active burning during our study period (informed by GFED-3). Once emitted the tracer is left to disperse. We assume a constant chemical lifetime of 60 days from the oxidation by OH, corresponding to an OH concentration of 1.9×10^6 molec cm^{-3}. At the end of a 31 day simulation

ACPD
14, 8723–8752, 2014

for July, say, we have 31 tracers. The age of each tracer is simply the number of days since the start of the run minus the tracer number (not value).

To account for older air being subject to more dispersion than younger air we define an effective age of air $\overline{A}$:

$$\overline{A} = \frac{\sum_i A_i L_{\mathrm{M},i} L_{\mathrm{C},i}}{\sum_i L_{\mathrm{M},i} L_{\mathrm{C},i}}, \quad (1)$$

which represents a weighted mean of the age of each tracer A_i, the value of each tracer $L_{\mathrm{M},i}$ that is a measure of atmospheric mixing processes, and the chemical lifetime of each tracer $L_{\mathrm{C},i}$. More generally, we can extend this formulation to include other sink terms such as, for example, dry and wet deposition. For $L_{\mathrm{C},i}$ we assume a constant chemical lifetime of 60 days as described above. This method does not account for the magnitude of CO emitted from any fire, regardless of its size.

For this paper, calculating $\overline{A}$ allows us to quantify the age of emissions intercepted during BORTAS-B, providing additional information to interpret the chemical signature of the sampled air masses. It also allows us to determine whether the air masses intercepted during BORTAS-B were representative of that summer and of a similar period from preceding years.

3 Results

3.1 Statistical analysis of BORTAS-B CO data

Figure 2 shows the mean statistics of the model and observed CO concentrations during BORTAS-B. Similar mean and median values of observed CO suggests the data are not skewed. This is supported by the mean model minus observed CO residuals of 0.5 ppb and a median of 3.1 ppb. We find the model has a positive bias below observations of 100 ppb and a negative bias for observations > 300 ppb. The largest

ACPD
14, 8723–8752, 2014

discrepancies between the model and the observations generally occur at the largest values of CO. The 99th percentile value for model and observed CO concentrations are 393 ppb and 423 ppb, respectively. The median (most frequent) observed CO is 80–120 ppb and is consistent with background CO measurements during the NASA ARCTAS-B campaign (Arctic Research of the Composition of the Troposphere from Aircraft and Satellites, Jacob et al., 2010). The largest observed CO concentrations during BORTAS-B are larger than the CO observed during ARCTAS-B (Liang et al., 2011). Figure 3 shows that the relative model error ((model minus observation)/model) is typically within ±0.3 but has a range of ±1.0. The model has a negative bias between the surface and 900 hPa and between 850 hPa and 700 hPa, reflecting the outflow of anthropogenic and biomass burning pollution, respectively. We find that the model has a some level of skill (r = 0.45) at reproducing the observed CO variability, averaged on the model grid, during BORTAS-B (not shown).

3.2 Tagged CO model output

Table 1 shows the tagged model analysis sampled at the times and locations of the BORTAS-B CO measurements. The largest source of CO and the largest source of CO variability during BORTAS was from NE North American biomass burning, as expected. There are also large but much less variable contributions from the background (air older than JJA) and from the oxidation of methane and NMVOCs. CO produced by CH_4 oxidation typically contributes around 30 % to global concentrations (Duncan et al., 2007).

Figure 4 shows the mean JJA model contributions of total surface CO from different geographically based sources for 2008–2011. The contribution from biomass burning over NW North America is broadly constant from year to year, although the distribution of the fires varies substantially, with Alaska playing a dominant role only in 2009 during our study period. The magnitude and the distribution of fossil fuel emissions from NE North America (predominately the NE USA) appear reasonably consistent over the four years, with emissions generally travelling up the eastern seaboard with eventual

ACPD
14, 8723–8752, 2014

outflow to the Atlantic ocean close to Halifax, Nova Scotia. Similar to North America, Siberian biomass burning has substantial spatial variability from year to year, with their location playing a key role in determining their eventual impact on North America and Europe. During 2010 the largest CO concentrations originated from East Siberia and spread across the Northern Hemisphere. In contrast, during BORTAS-B in 2011 most of the fire activity was further SW and had less of an impact over eastern Canada. Fires from mid-Siberia had a larger influence on total CO during 2008–2009, with very little activity during 2010–2011. There is a consistently small source from fossil fuel combustion from East Asia (not shown), peaking at around 400 ppb over China but quickly dropping off to around 10 ppb by the time it has crossed the Pacific. Differences between Figs. 4 and 9 from Palmer et al. (2013), also showing polar CO concentrations during BORTAS-B, is due to different biomass burning inventories. Here, we use GFED-3 (see above) and Palmer et al. (2013) used the Fire Locating and Modeling of Burning Emissions inventory (Reid et al., 2009).

Figure 5 shows that biomass burning from the NW North America is still a dominant factor in the variability of total CO in the free troposphere. During 2010, these fires contributed around 50 ppb of CO into the upper troposphere causing widespread pollution during July. Typically these emissions contribute about 10 ppb of CO over Europe. Contributions from east and mid Siberia appear to be consistent over the four years except during 2010 when there is very little material transported into the free troposphere. In general, the magnitude and distribution of the fossil fuel source is consistent across the four years with weather systems lifting up surface emission to the free troposphere.

The widespread and persistent source of CO (approximately 10 ppb) from Asian anthropogenic sources over the Northern Hemisphere (not shown) agrees with the ARCTAS-A study (Fisher et al., 2010) and ARCTAS-B (Bian et al., 2013). Relative to ARCTAS-A, BORTAS-B generally shows a much larger contribution to the total CO from boreal biomass burning, reflecting the timing of ARCTAS-A in April 2008 before the beginning of the main fire season. For JJA 2008–2011 we find boreal biomass burning represents a significant contribution to the total surface CO over the Western

ACPD
14, 8723–8752, 2014

Arctic region defined as 50–90° N, 170–40° W, following Bian et al. (2013). Analysis of ARCTAS-B data showed that boreal biomass burning contributed approximately 25 % of CO in this region during July 2008 (Bian et al., 2013). We find boreal biomass burning contributes 25–45 % of the total CO for the defined Western Arctic region for all years, peaking at > 90 % of the total CO over intense burning areas. During 2008 we find our results are broadly consistent with Bian et al. (2013) but at the lower end of their range. The discrepancy between these results is likely due to using different emission inventories, with Bian et al. (2013) using the Quick Fire Emissions Database.

3.3 Age of air

Figure 6 shows the mean model statistics for the age of air for July 2008–2011 at 95° W and 50°, averaged over 40–70° N, representing the approximate western and eastern boundaries of the measurements sampled during BORTAS-B. We consider four altitude bins, corresponding to the boundary layer (0–2 km), lower and mid troposphere (2–4 km and 4–6 km, respectively), and upper troposphere (> 6 km). At the western boundary, emissions have a median age of approximately 6–8 days, with the exception of 2009 when air is typically 8 days old, ranging from 1 to 20 days. We find the older age of emissions during 2009 is due to fewer fires along the western boundary with values more representative of air travelling from Alaska and further afield. Air sampled at the eastern boundary is older, as expected with the exception of the upper troposphere (> 6 km) which shows similar medians from the western boundary to the eastern boundary. The eastern boundary has a median age of 11–13 days and a range of 2–23 days. The difference in the age of air between the two boundaries decreases with altitude, where above 4 km ages are indistinguishable due to air being more well-mixed and influenced by emissions outside of the domain. The age of emissions clearly gets older moving towards the Atlantic for all years except 2009, when the median age is 10 days, which is due to the fires during this year being earlier in the season and located in Alaska. There was very little biomass burning activity in mid-Canada for 2009. Emissions tend to be older at 50° W at lower altitudes (not shown).

ACPD
14, 8723–8752, 2014

This may be a result from fresher emissions getting lofted higher into the atmosphere as they travel. Figure 6 also shows that the median age of emissions (6 days) sampled during BORTAS-B falls within the range of model emission ages at 95° W, with the majority of measurements taken 65°–40° W. We find a similar observed median age for all altitudes, which is typically lower than the model free troposphere. This bias towards younger ages reflects the sampling strategy of BORTAS-B that was to intercept fresh biomass burning plumes.

Figure 7 shows an example of the effective age of emissions on 20 July 2011, which is used as a case study in other BORTAS studies (e.g., Griffin et al., 2013; Franklin et al., 2014). The longitudinal cross section shows fresh emissions from the Thunder Bay region, peaking on the 16–17 July, that eventually age as they are transported eastwards. When they were intercepted by the surface measurements over Toronto (43.70° N, 69.40° W) (Griffin et al., 2013) and Halifax (44.6° N, 63.59° W) (Franklin et al., 2014) emissions are typically 5–7 days old. Figure 7 shows the transported air, intercepted at 63° W, is composed of a young plume (3–5 days old) surrounded by older air (7 days old) over 47–55° N. Griffin et al. (2013) showed using HYSPLIT backtrajectories (Draxler and Hess, 1998) that observed CO on 19–21 July 2011 originated over NW Ontario and eastern Siberia, and approximated associated travel times of 1–2 days and 1 week, respectively.

Figure 8 shows the mean statistics of the age of emissions intercepted during BORTAS-B is generally consistent with the associated median photochemical age, determined using NMVOC ratios, of six days (Parrington et al., 2013). The photochemical ages range 0–16 days while the physically-based ages range 2–14 days. There are substantial differences between the photochemical and physical ages for each flight. Figure 9 shows that $\overline{A}$ minus photochemical age ($\Delta\tau$) have distinct frequency distributions within and outwith plumes. Within plumes, the distribution peaks at $\Delta\tau$ = 3–5 days (median 2.17 days), while outwith plumes there is a reasonably flat distribution tailing off where $|\Delta\tau| > 5$ days. We find no significant difference to our results if we average the photochemical ages onto the model grid prior to the analysis. Figure 9 shows that CO

ACPD
14, 8723–8752, 2014

within plumes peaks where $\Delta\tau$ is also 2–4 days, corresponding to a mean fractional difference of 39 % and a median fractional difference of 50 %, while there is a weaker relationship between $\Delta\tau$ outwith plumes, corresponding to a mean fractional difference of −11 % and a median of −12 %. Figure 9 also shows that $\Delta\tau$ increases with $\overline{A}$ within plumes ($r^2 = 0.60$) from close to zero at 3–4 days to > 5 days for plumes older than 10 days. There is only a weak relationship between these two age variables outwith plumes ($r^2 = 0.23$).

4 Concluding remarks

We used the GEOS-Chem global atmospheric chemistry model to interpret observed variations of CO taken during the BORTAS-B aircraft campaign over eastern Canada in July–August 2011. We showed that the model has some skill at reproducing the mean observed statistics in the lower and free troposphere ($r = 0.45$), with a mean difference of −0.1 ppb and a median of 2.0 ppb. The distribution of these residuals has a high kurtosis, with the majority of residuals within 50 ppb of the mean value. The model has a negative bias below observed values of 100 ppb and a positive bias above 300 ppb. We found that the larger differences between the model and the observations is in the mid troposphere, where we found pyrogenic CO peaked. We have attributed these residuals to model errors in emission inventories and the sub-grid scale vertical mixing of pyrogenic material lofted by surface heating due to fires.

Using a linearly-decomposed version of the model we found that most of the observed variability in CO concentration during BORTAS-B was due to Canadian biomass burning, as expected, with a smaller contribution from Siberian biomass burning and NE North American fossil fuel combustion. We used the model to put BORTAS-B into the wider temporal context of 2008–2011. We found that North American biomass burning is broadly constant (45 % of total CO) over this period although the spatial distribution of fires varies substantially. The variation of Siberian biomass burning is more extreme with large contributions to total CO over North American during some years

ACPD
14, 8723–8752, 2014

(2008–2009) and very little activity in other years (2010–2011), reflecting the spatial extent and geographical position of the fires. Based on our analysis of the source contributions to North American CO over during the (limited) four-year period we conclude that BORTAS-B (2011) was not anomalous.

Previous work has shown that ozone production within biomass burning plumes can be described using photochemical ageing (Parrington et al., 2013). In this paper we described a new Eulerian method to quantify the effective age of emissions, taking into account mixing and chemical decay of emitted air masses of varying age. We found that during BORTAS-B, the age of emissions intercepted over Halifax, Nova Scotia are typically 4–11 days old but occasionally as young as two days, corresponding well to analysis of concurrent ground-based observations at the Dalhousie ground station in Halifax, NS (Gibson et al., 2013). We found our Eulerian approach led to ages of a day older than the NOAA HYSPLIT Lagrangian back trajectory model during the 19–21 July 2011 when ground-based observations reported elevated concentrations due to biomass burning (Gibson et al., 2013; Griffin et al., 2013; Franklin et al., 2014). We attributed this difference in age to our method accounting for older air masses that are not explicitly considered by HYSPLIT. We compared the physical ages calculated using our method to the corresponding photochemical ages, using ratios of NMVOCs (Parrington et al., 2013), and found that the physical age is typically 1–5 days older. We find that the median difference between the age measures in plumes (defined as $CH_3CN > 150$ ppt) peaks at 3–5 days, compared to a muted distribution for background CO concentrations, corresponding to a chemical retardation of 50 %. We also found that in plumes $\Delta\tau$ increased with physical age ($r^2 = 0.60$), which was much less pronounced outwith plumes ($r^2 = 0.23$). Based on $\Delta\tau$ within and outwith plumes and on a strong relationship between CO and, for example, black carbon aerosol during BORTAS-B ($r^2 > 0.7$, personal communication, Jonathan Taylor, University of Manchester, 2014) we hypothesize that $\Delta\tau$ variations provide evidence that pyrogenic aerosols slow down the plume photochemistry for many days downwind from the point of burning.

ACPD
14, 8723–8752, 2014

Previous work using a photochemical model has shown that the ozone tendency of Alaskan forest fire plumes observed over the North Atlantic during 2004 was consistent with a reduced photolysis rate of approximately 20 % that could be due to aerosol loading within/above these plumes (Real et al., 2007). Our analysis of physical vs. photochemical age suggests a larger retardation to the plume photochemistry. One important counter argument to our analysis of $\Delta\tau$ that could reconcile the physical and photochemical ages is that the photochemical age could have a negative bias. The method, described in detail by Parrington et al. (2013), relies on variation of NMVOC ratios that have different chemical lifetimes against oxidation by OH. The lifetime calculation is anchored by an assumption of a constant OH concentration. The BORTAS-B data analysis assumed an OH concentration of 2×10^6 molec cm^{-3} that was chosen to be representative of a northern midlatitude summertime OH concentration (Spivakovsky et al., 2000). Halving the assumed OH concentration would double the photochemical age and doubling OH would halve the photochemical age. For many flights the median physical age is substantial higher than the photochemical age.

The Eulerian effective mean age does not consider the size of the fire and the amount of CO that is emitted. While this will not affect the age calculation it may complicate the interpretation of data. If, for example, old, high-CO air masses mix with young, low-CO air masses our method will assign more weight to the younger air mass and a stronger attribution to the observed CO variability. We have tried to minimize this issue by using a fixed chemical decay but some residual of this issue will unavoidably remain. Other measures of age inferred from Lagrangian back trajectories, say, will suffer from similar problems and in some circumstances be more problematic if the mixing of different air masses is not considered.

Accounting for biomass burning in regional air quality budgets downwind of fires presents a number of challenges, not least due to the ability of models to predict where plume chemistry will result in net production of O_3. It is well established that this production is a function of the pyrogenic emissions (themselves a function of many environmental variables), the associated vertical mixing and transport pathways, and

ACPD
14, 8723–8752, 2014

the photochemical environment. Using BORTAS-B we have only inferred that aerosols have slowed photochemical ageing of plumes but there is insufficient data to characterize directly how the aerosols have affected the photochemical environment within the plume as a function of time. Further studies of similar pyrogenic plumes should include a full suite of aerosol and radiation instruments in addition to gas-phase atmospheric chemistry instruments. This kind of integrative analysis will become progressively more important as we analyze more complex environments such as megacities where there is typically a mix of biogenic, anthropogenic, and pyrogenic material determining ozone photochemistry.

Acknowledgements. This research was supported by the Natural Environment Research Council under grant number NE/F017391/1. DF acknowledges NERC studentship NE/K500835/1. PIP acknowledges support from his Philip Leverhulme Prize and his Royal Society Wolfson Research Merit Award. DF and PIP designed the numerical calculations, performed the analysis, and wrote the paper; PIP was also the principal BORTAS mission scientist. MP was a mission scientist on BORTAS, and provided the photochemical ages and comments on the paper.

References

Akagi, S. K., Yokelson, R. J., Wiedinmyer, C., Alvarado, M. J., Reid, J. S., Karl, T., Crounse, J. D., and Wennberg, P. O.: Emission factors for open and domestic biomass burning for use in atmospheric models, Atmos. Chem. Phys., 11, 4039–4072, doi:10.5194/acp-11-4039-2011, 2011. 8725

Bey, I., Jacob, D. J., Yantosca, R. M., Logan, J. A., Field, B. D., Fiore, A. M., Li, Q., Liu, H. Y., Mickley, L. J., and Schultz, M. G.: Global modeling of tropospheric chemistry with assimilated meteorology: model description and evaluation, J. Geophys. Res., 106, 23073, doi:10.1029/2001JD000807, 2001. 8726

Bian, H., Colarco, P. R., Chin, M., Chen, G., Rodriguez, J. M., Liang, Q., Blake, D., Chu, D. A., da Silva, A., Darmenov, A. S., Diskin, G., Fuelberg, H. E., Huey, G., Kondo, Y., Nielsen, J. E., Pan, X., and Wisthaler, A.: Source attributions of pollution to the Western Arctic during the

ACPD
14, 8723–8752, 2014

NASA ARCTAS field campaign, Atmos. Chem. Phys., 13, 4707–4721, doi:10.5194/acp-13-4707-2013, 2013. 8730, 8731

Draxler, R. R. and Hess, G. D.: An overview of the HYSPLIT 4 modeling system of trajectories, dispersion, and deposition, Aust. Meteorol. Mag., 47, 295–308, 1998. 8732

Duncan, B. N., Logan, J. A., Bey, I., Megretskaia, I. A., Yantosca, R. M., Novelli, P. C., Jones, N. B., and Rinsland, C. P.: Global budget of CO, 1988–1997: source estimates and validation with a global model, J. Geophys. Res., 112, D22301, doi:10.1029/2007JD008459, 2007. 8725, 8726, 8729

Feng, L., Palmer, P. I., Bösch, H., and Dance, S.: Estimating surface CO_2 fluxes from space-borne CO_2 dry air mole fraction observations using an ensemble Kalman Filter, Atmos. Chem. Phys., 9, 2619–2633, doi:10.5194/acp-9-2619-2009, 2009. 8727

Fisher, J. A., Jacob, D. J., Purdy, M. T., Kopacz, M., Le Sager, P., Carouge, C., Holmes, C. D., Yantosca, R. M., Batchelor, R. L., Strong, K., Diskin, G. S., Fuelberg, H. E., Holloway, J. S., Hyer, E. J., McMillan, W. W., Warner, J., Streets, D. G., Zhang, Q., Wang, Y., and Wu, S.: Source attribution and interannual variability of Arctic pollution in spring constrained by aircraft (ARCTAS, ARCPAC) and satellite (AIRS) observations of carbon monoxide, Atmos. Chem. Phys., 10, 977–996, doi:10.5194/acp-10-977-2010, 2010. 8727, 8730

Franklin, J. E., Drummond, J. R., Griffin, D., Pierce, J. R., Waugh, D. L., Palmer, P. I., Parrington, M., Lee, J. D., Lewis, A. C., Rickard, A. R., Taylor, J. W., Allan, J. D., Coe, H., Walker, K. A., Chisholm, L., Duck, T. J., Hopper, J. T., Blanchard, Y., Gibson, M. D., Curry, K. R., Sakamoto, K. M., Lesins, G., Dan, L., Kliever, J., and Saha, A.: A case study of aerosol depletion in a biomass burning plume over Eastern Canada during the 2011 BORTAS field experiment, Atmos. Chem. Phys. Discuss., 14, 3395–3426, doi:10.5194/acpd-14-3395-2014, 2014. 8732, 8734

Gerbig, C., Schmitgen, S., Kley, D., Volz-Thoms, A., Dewey, K., Haaks, D., and Volz-Thomas, A.: An improved fast-response vacuum-UV resonance fluorescence CO instrument, J. Geophys. Res., 104, 1699–1704, doi:10.1029/1998JD100031, 1999. 8726

Gibson, M. D., Pierce, J. R., Waugh, D., Kuchta, J. S., Chisholm, L., Duck, T. J., Hopper, J. T., Beauchamp, S., King, G. H., Franklin, J. E., Leaitch, W. R., Wheeler, A. J., Li, Z., Gagnon, G. A., and Palmer, P. I.: Identifying the sources driving observed $PM_{2.5}$ temporal variability over Halifax, Nova Scotia, during BORTAS-B, Atmos. Chem. Phys., 13, 7199–7213, doi:10.5194/acp-13-7199-2013, 2013. 8725, 8734

ACPD
14, 8723–8752, 2014

Giglio, L., Randerson, J. T., van der Werf, G. R., Kasibhatla, P. S., Collatz, G. J., Morton, D. C., and DeFries, R. S.: Assessing variability and long-term trends in burned area by merging multiple satellite fire products, Biogeosciences, 7, 1171–1186, doi:10.5194/bg-7-1171-2010, 2010. 8726

Gonzi, S., Feng, L., and Palmer, P. I.: Seasonal cycle of emissions of {CO} inferred from {MOPITT} profiles of {CO}: sensitivity to pyroconvection and profile retrieval assumptions, Geophys. Res. Lett., 38, L08813, doi:10.1029/2011GL046789 2011. 8726

Goode, J. G., Yokelson, R. J., Ward, D. E., Susott, R. A., Babbitt, R. E., Davies, M. A., and Hao, W. M.: Measurements of excess O_3, CO_2, CO, CH_4, C_2H_4, C_2H_2, HCN, NO, NH_3, HCOOH, CH_3 COOH, HCHO, and CH_3 OH in 1997 Alaskan biomass burning plumes by airborne Fourier transform infrared spectroscopy (AFTIR), J. Geophys. Res., 105, 22147, doi:10.1029/2000JD900287, 2000. 8724

Griffin, D., Walker, K. A., Franklin, J. E., Parrington, M., Whaley, C., Hopper, J., Drummond, J. R., Palmer, P. I., Strong, K., Duck, T. J., Abboud, I., Bernath, P. F., Clerbaux, C., Coheur, P.-F., Curry, K. R., Dan, L., Hyer, E., Kliever, J., Lesins, G., Maurice, M., Saha, A., Tereszchuk, K., and Weaver, D.: Investigation of CO, C_2H_6 and aerosols in a boreal fire plume over eastern Canada during BORTAS 2011 using ground- and satellite-based observations and model simulations, Atmos. Chem. Phys., 13, 10227–10241, doi:10.5194/acp-13-10227-2013, 2013. 8725, 8732, 8734

Guenther, A., Karl, T., Harley, P., Wiedinmyer, C., Palmer, P. I., and Geron, C.: Estimates of global terrestrial isoprene emissions using MEGAN (Model of Emissions of Gases and Aerosols from Nature), Atmos. Chem. Phys., 6, 3181–3210, doi:10.5194/acp-6-3181-2006, 2006. 8727

Jacob, D. J., Crawford, J. H., Maring, H., Clarke, A. D., Dibb, J. E., Emmons, L. K., Ferrare, R. A., Hostetler, C. A., Russell, P. B., Singh, H. B., Thompson, A. M., Shaw, G. E., McCauley, E., Pederson, J. R., and Fisher, J. A.: The Arctic Research of the Composition of the Troposphere from Aircraft and Satellites (ARCTAS) mission: design, execution, and first results, Atmos. Chem. Phys., 10, 5191–5212, doi:10.5194/acp-10-5191-2010, 2010. 8729

Jaffe, D. A., and Wigder, N. L.: Ozone production from wildfires: a critical review, Atmos. Environ., 51, 1–10, doi:10.1016/j.atmosenv.2011.11.063, 2012. 8725

Jones, D. B. A., Bowman, K. W., Palmer, P. I., Worden, J. R., Jacob, D. J., Hoffman, R. N., Bey, I., and Yantosca, R. M.: Potential of observations from the tropospheric emission spectrometer

ACPD
14, 8723–8752, 2014

to constrain continental sources of carbon monoxide, J. Geophys. Res. Atmos., 108, 4789, doi:10.1029/2003JD003702, 2003. 8727

Koppmann, R., von Czapiewski, K., and Reid, J. S.: A review of biomass burning emissions, part I: gaseous emissions of carbon monoxide, methane, volatile organic compounds, and nitrogen containing compounds, Atmos. Chem. Phys. Discuss., 5, 10455–10516, doi:10.5194/acpd-5-10455-2005, 2005. 8724

Le Breton, M., Bacak, A., Muller, J. B. A., O'Shea, S. J., Xiao, P., Ashfold, M. N. R., Cooke, M. C., Batt, R., Shallcross, D. E., Oram, D. E., Forster, G., Bauguitte, S. J.-B., Palmer, P. I., Parrington, M., Lewis, A. C., Lee, J. D., and Percival, C. J.: Airborne hydrogen cyanide measurements using a chemical ionisation mass spectrometer for the plume identification of biomass burning forest fires, Atmos. Chem. Phys., 13, 9217–9232, doi:10.5194/acp-13-9217-2013, 2013. 8725

Lewis, A. C., Evans, M. J., Hopkins, J. R., Punjabi, S., Read, K. A., Purvis, R. M., Andrews, S. J., Moller, S. J., Carpenter, L. J., Lee, J. D., Rickard, A. R., Palmer, P. I., and Parrington, M.: The influence of biomass burning on the global distribution of selected non-methane organic compounds, Atmos. Chem. Phys., 13, 851–867, doi:10.5194/acp-13-851-2013, 2013. 8725

Liang, Q., Rodriguez, J. M., Douglass, A. R., Crawford, J. H., Olson, J. R., Apel, E., Bian, H., Blake, D. R., Brune, W., Chin, M., Colarco, P. R., da Silva, A., Diskin, G. S., Duncan, B. N., Huey, L. G., Knapp, D. J., Montzka, D. D., Nielsen, J. E., Pawson, S., Riemer, D. D., Weinheimer, A. J., and Wisthaler, A.: Reactive nitrogen, ozone and ozone production in the Arctic troposphere and the impact of stratosphere-troposphere exchange, Atmos. Chem. Phys., 11, 13181–13199, doi:10.5194/acp-11-13181-2011, 2011. 8729

Murphy, J. G., Oram, D. E., and Reeves, C. E.: Measurements of volatile organic compounds over West Africa, Atmos. Chem. Phys., 10, 5281–5294, doi:10.5194/acp-10-5281-2010, 2010. 8726

Olivier, J. G. J., Bloos, J. P. J., Berdowski, J. J. M., Visschedijk, A. J. H., and Bouwman, A. F.: A 1990 global emission inventory of anthropogenic sources of carbon monoxide on 1° × 1° developed in the framework of EDGAR/GEIA, Chemosph. Glob. Chang. Sci., 1, 1–17, doi:10.1016/S1465-9972(99)00019-7, 1999. 8726

O'Shea, S. J., Allen, G., Gallagher, M. W., Bauguitte, S. J.-B., Illingworth, S. M., Le Breton, M., Muller, J. B. A., Percival, C. J., Archibald, A. T., Oram, D. E., Parrington, M., Palmer, P. I., and Lewis, A. C.: Airborne observations of trace gases over boreal Canada during BORTAS:

ACPD
14, 8723–8752, 2014

campaign climatology, air mass analysis and enhancement ratios, Atmos. Chem. Phys., 13, 12451–12467, doi:10.5194/acp-13-12451-2013, 2013. 8725

Palmer, P. I., Jacob, D. J., Jones, D. B. A., Heald, C. L., Yantosca, R. M., and Logan, J. A.: Inverting for emissions of carbon monoxide from Asia using aircraft observations over the western Pacific, J. Geophys. Res., 108, 8828, doi:10.1029/2003JD003397, 2003. 8727

Palmer, P. I., Suntharalingam, P., Jones, D. B. A., Jacob, D. J., Streets, D. G., Fu, Q., Vay, S. A., and Sachse, G. W.: Using CO_2 : CO correlations to improve inverse analyses of carbon fluxes, J. Geophys. Res., 111, D12318, doi:10.1029/2005JD006697, 2006. 8727

Palmer, P. I., Parrington, M., Lee, J. D., Lewis, A. C., Rickard, A. R., Bernath, P. F., Duck, T. J., Waugh, D. L., Tarasick, D. W., Andrews, S., Aruffo, E., Bailey, L. J., Barrett, E., Bauguitte, S. J.-B., Curry, K. R., Di Carlo, P., Chisholm, L., Dan, L., Forster, G., Franklin, J. E., Gibson, M. D., Griffin, D., Helmig, D., Hopkins, J. R., Hopper, J. T., Jenkin, M. E., Kindred, D., Kliever, J., Le Breton, M., Matthiesen, S., Maurice, M., Moller, S., Moore, D. P., Oram, D. E., O'Shea, S. J., Owen, R. C., Pagniello, C. M. L. S., Pawson, S., Percival, C. J., Pierce, J. R., Punjabi, S., Purvis, R. M., Remedios, J. J., Rotermund, K. M., Sakamoto, K. M., da Silva, A. M., Strawbridge, K. B., Strong, K., Taylor, J., Trigwell, R., Tereszchuk, K. A., Walker, K. A., Weaver, D., Whaley, C., and Young, J. C.: Quantifying the impact of BOReal forest fires on Tropospheric oxidants over the Atlantic using Aircraft and Satellites (BORTAS) experiment: design, execution and science overview, Atmos. Chem. Phys., 13, 6239–6261, doi:10.5194/acp-13-6239-2013, 2013. 8725, 8726, 8730, 8749

Parrington, M., Palmer, P. I., Henze, D. K., Tarasick, D. W., Hyer, E. J., Owen, R. C., Helmig, D., Clerbaux, C., Bowman, K. W., Deeter, M. N., Barratt, E. M., Coheur, P.-F., Hurtmans, D., Jiang, Z., George, M., and Worden, J. R.: The influence of boreal biomass burning emissions on the distribution of tropospheric ozone over North America and the North Atlantic during 2010, Atmos. Chem. Phys., 12, 2077–2098, doi:10.5194/acp-12-2077-2012, 2012. 8725, 8726

Parrington, M., Palmer, P. I., Lewis, A. C., Lee, J. D., Rickard, A. R., Di Carlo, P., Taylor, J. W., Hopkins, J. R., Punjabi, S., Oram, D. E., Forster, G., Aruffo, E., Moller, S. J., Bauguitte, S. J.-B., Allan, J. D., Coe, H., and Leigh, R. J.: Ozone photochemistry in boreal biomass burning plumes, Atmos. Chem. Phys., 13, 7321–7341, doi:10.5194/acp-13-7321-2013, 2013. 8732, 8734, 8735

Real, E., Law, K. S., Weinzierl, B., Fiebig, M., Petzold, A., Wild, O., Methven, J., Arnold, S., Stohl, A., Huntrieser, H., Roiger, A., Schlager, H., Stewart, D., Avery, M., Sachse, G., Brow-

ACPD
14, 8723–8752, 2014

ell, E., Ferrare, R., and Blake, D.: Processes influencing ozone levels in Alaskan forest fire plumes during long-range transport over the North Atlantic, J. Geophys. Res., 112, D10S41, doi:10.1029/2006JD007576, 2007. 8735

Reid, J. S., Hyer, E. J., Prins, E. M., Westphal, D. L., Zhang, J., Wang, J., Christopher, S. A., Curtis, C. A., Schmidt, C. C., Eleuterio, D. P., Richardson, K. A., and Hoffman, J. P.: Global monitoring and forecasting of biomass-burning smoke: description of and lessons from the Fire Locating and Modeling of Burning Emissions (FLAMBE) Program, IEEE J. Sel. Top. Appl. Earth Obs. Remote Sens., 2, 144–162, doi:10.1109/JSTARS.2009.2027443, 2009. 8730

Spivakovsky, C. M., Logan, J. A., Montzka, S. A., Balkanski, Y. J., Foreman-Fowler, M., Jones, D. B. A., Horowitz, L. W., Fusco, A. C., Brenninkmeijer, C. A. M., Prather, M. J., Wofsy, S. C., and McElroy, M. B.: Three-dimensional climatological distribution of tropospheric OH: Update and evaluation, J. Geophys. Res.-Atmos., 105, 8931–8980, doi:10.1029/1999JD901006, 2000. 8735

Tereszchuk, K. A., Moore, D. P., Harrison, J. J., Boone, C. D., Park, M., Remedios, J. J., Randel, W. J., and Bernath, P. F.: Observations of peroxyacetyl nitrate (PAN) in the upper troposphere by the Atmospheric Chemistry Experiment-Fourier Transform Spectrometer (ACE-FTS), Atmos. Chem. Phys., 13, 5601–5613, doi:10.5194/acp-13-5601-2013, 2013. 8725

ACPD
14, 8723–8752, 2014

Table 1. Contribution of CO from geographical sources averaged over all BORTAS-B flights, lumping all other contributions < 2 ppb into "Other". Background refers to any residual CO before the beginning of the BORTAS-B period.

Tracer Source	Mean (ppb)	Std Dev (ppb)
NE USA and Canada Biomass Burning	30.9	66.3
East Asian Fossil Fuel	11.4	3.2
North East American Fossil Fuel	6.0	11.6
NW USA and Canada Biomass Burning	5.5	3.8
North West American Fossil Fuel	3.2	1.8
Eastern Siberia Biomass Burning	3.1	4.6
Other	8.2	1.3
Methane and NMVOCS	24.4	2.7
Background	32.1	7.0

ACPD
14, 8723–8752, 2014

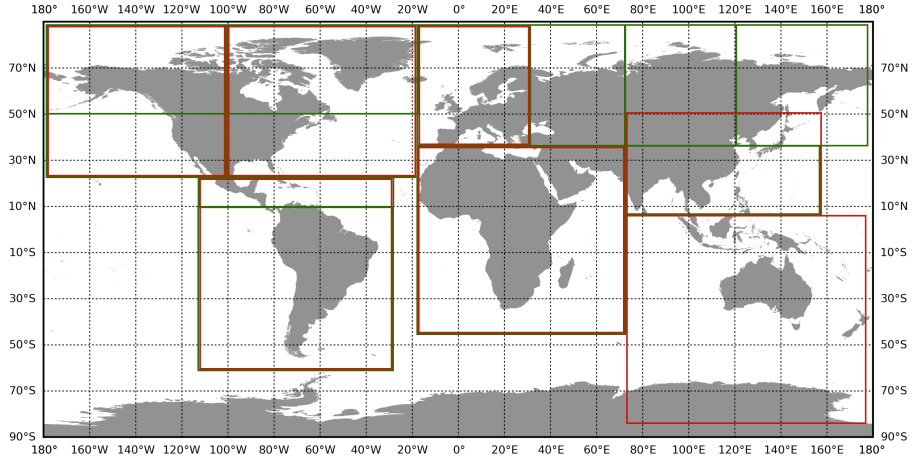

Fig. 1. Source regions for the tagged CO simulation. Regions outlined in red denote fossil fuel tagged tracers and regions outlined in green refer to biomass burning tagged tracers.

ACPD
14, 8723–8752, 2014

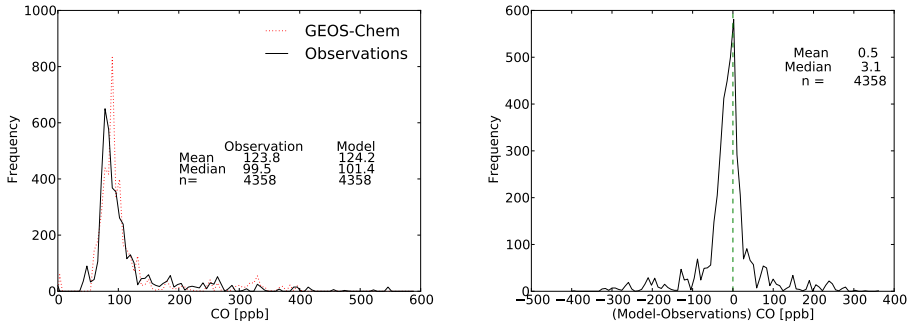

Fig. 2. Statistical comparison of model and observed CO from BORTAS-B. The observations have been averaged over the 2° × 2.5° model grid. Left panel shows the frequency distributions and the right panel shows the frequency distribution of the model minus observed CO residuals. Mean and median values are shown inset of each panel.

ACPD
14, 8723–8752, 2014

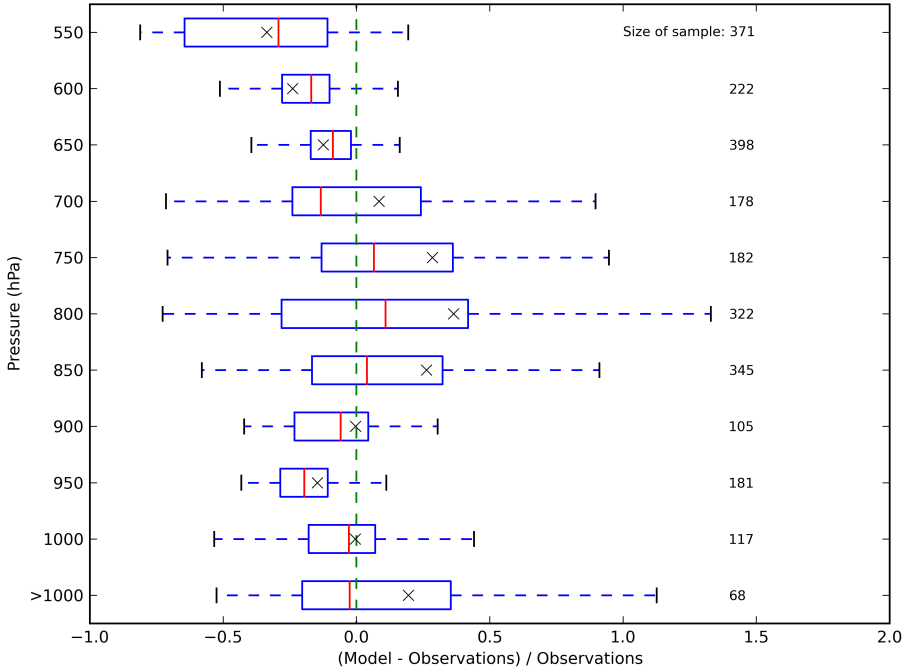

Fig. 3. Relative model error in the GEOS-Chem simulation of CO during BORTAS-B as a function of altitude described by the box and whiskers approach. The red line and grey cross denotes the median and mean values, respectively.

ACPD
14, 8723–8752, 2014

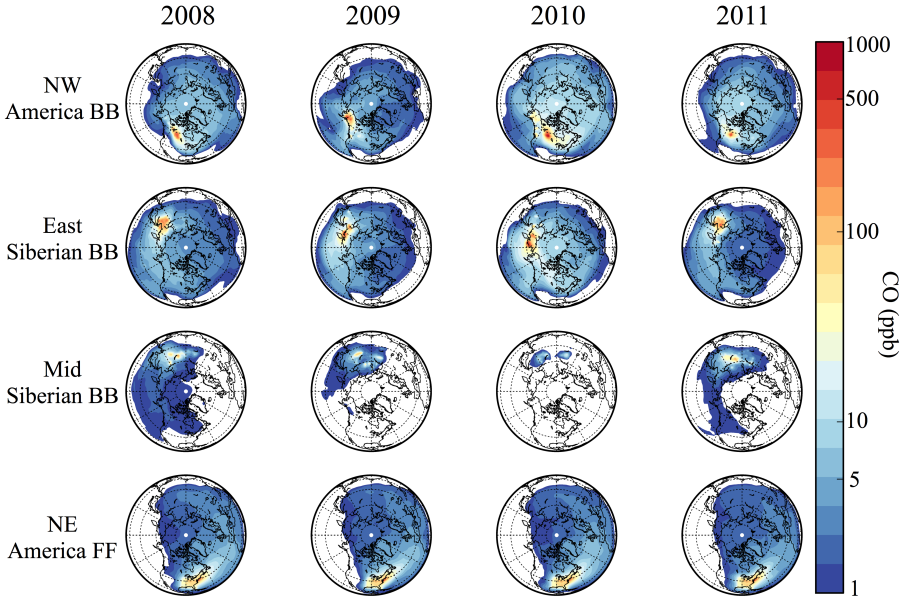

Fig. 4. Mean June–August GEOS-Chem model surface CO concentrations (ppb) from the four largest sources over the Northern Hemisphere for 2008–2011. Individual contributions (Fig. 1) are from NW North America biomass burning emissions (first row), NE North America fossil fuel (second row), East Siberia biomass burning (third row), and mid-Siberia biomass burning (bottom row).

ACPD
14, 8723–8752, 2014

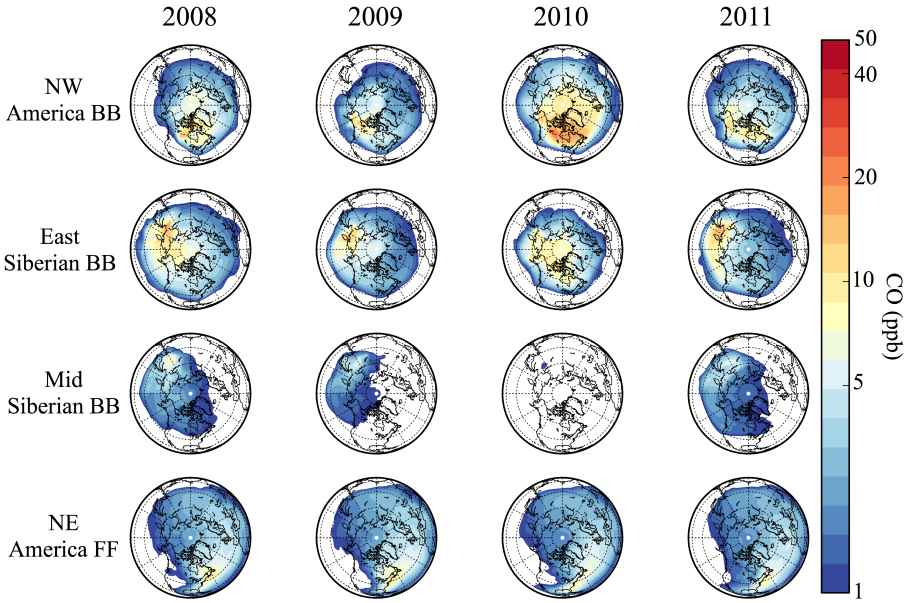

Fig. 5. Same as Fig. 4 but at 4 km altitude. Note the different upper limit to the colour bar.

ACPD
14, 8723–8752, 2014

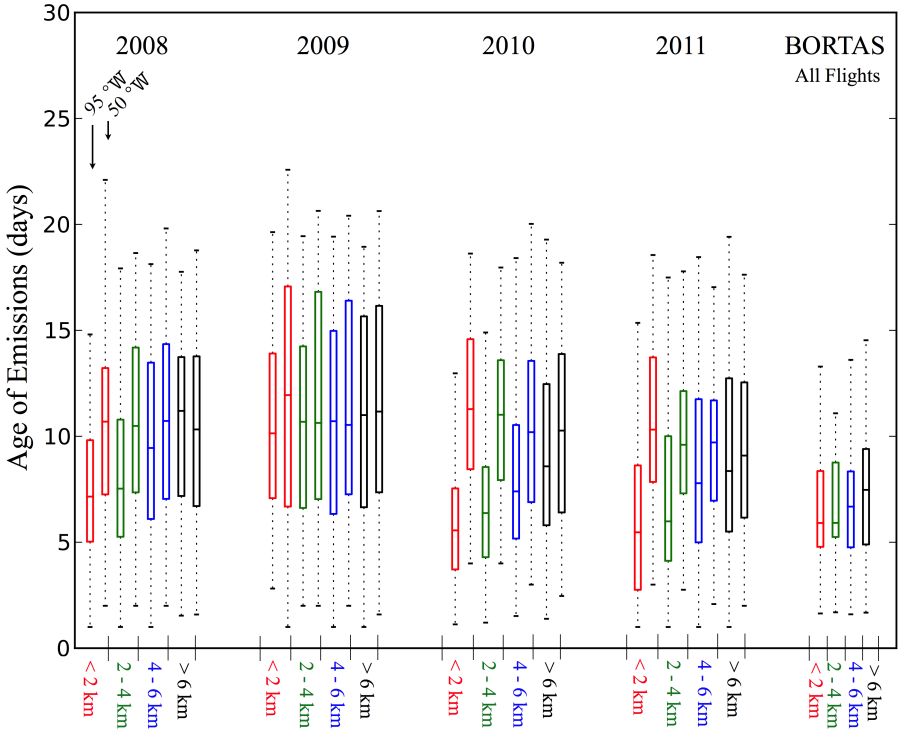

Fig. 6. Box and whiskers plot showing the mean age of emissions for different altitudes (< 2 km, 2–4 km, 4–6 km, and > 6 km) at the longitudinal boundaries of the BORTAS-B domain (45° N–60° N, 95° W–50° W) during July 2008, 2009, 2010, 2011, and for the model sampled along the BORTAS-B flights. Within the box, the upper, middle, and lower horizontal bars denote the first quartile, the median, and the third quartile. The full range of data is shown by the whiskers.

ACPD
14, 8723–8752, 2014

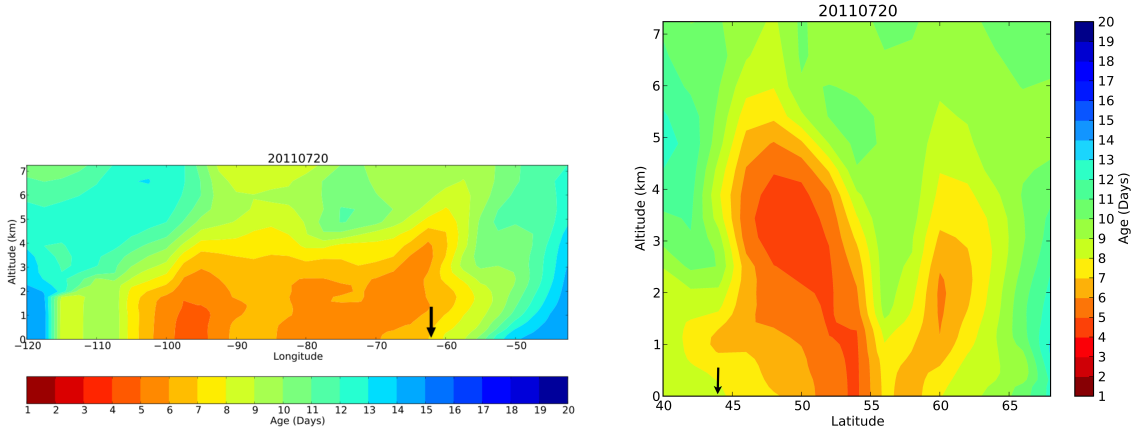

Fig. 7. Age of emissions on 20 July 2011 (left) from 120–40° W and 0–7 km, averaged over 45–55° N; and (right) 40–70° N and 0–7 km at 63° W, the same longitude as the Dalhousie University, Halifax, NS surface measurements (Palmer et al., 2013). Location of Dalhousie University is shown by the black arrow.

ACPD
14, 8723–8752, 2014

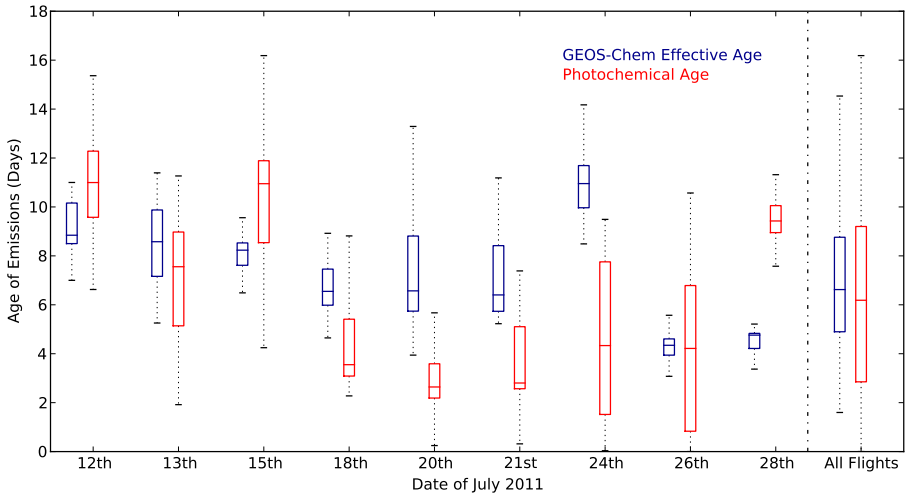

Fig. 8. Box and whiskers plot of the age of air observed during individual BORTAS-B aircraft flights using photochemical age from BORTAS-B data (red) and effective age $\overline{A}$ using the GEOS-Chem model (blue). The box and whiskers plot for all flights are shown on the last two right columns. Within the box, the upper, middle, and lower horizontal bars denote the first quartile, the median, and the third quartile. The full range of data is shown by the whiskers.

ACPD
14, 8723–8752, 2014

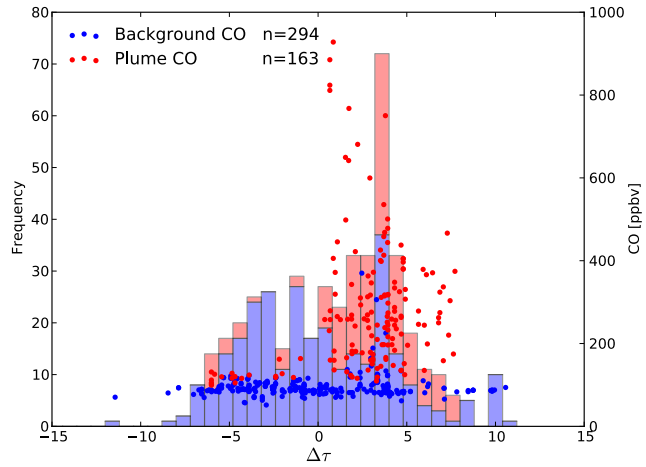

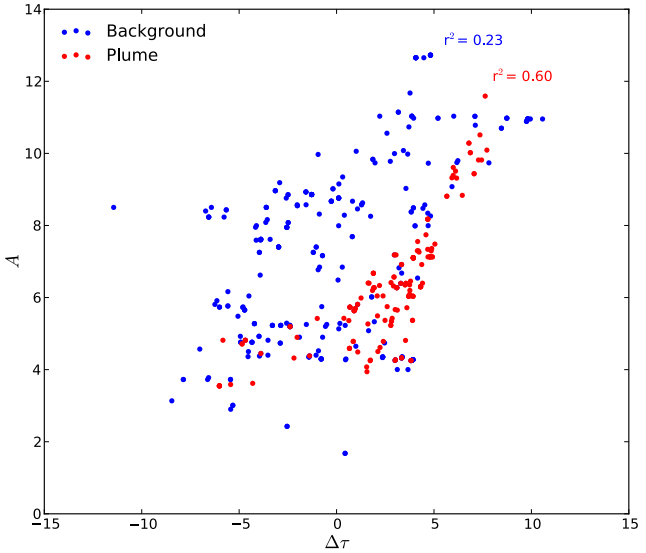

ACPD
14, 8723–8752, 2014

Biomass burning air masses during BORTAS

D. P. Finch et al.

Fig. 9. Top panel: frequency of effective age $\overline{A}$ minus photochemical age (days, left axis) and CO concentration (ppb, right axis). The number of measurements n for each classification are shown inset. Bottom panel: scatterplot of $\Delta\tau$ and $\overline{A}$. Red dots denote CO concentrations within a plume ($CH_3CN > 150$ ppt) and the blue dots denote CO concentrations outwith a plume.

ACPD
14, 8723–8752, 2014